An adaptive remeshing strategy for viscoelastic fluid flow simulations

Guénette, R.; Fortin, A.; Kane, A.; Hétu, J.-F.

Publisher’s version / Version de l'éditeur:
https://doi.org/10.1016/j.jnnfm.2007.11.009
Journal of Non-Newtonian Fluid Mechanics, 153, 1, pp. 34-45, 2007-12-08

ELSEVIER

J. Non-Newtonian Fluid Mech. 153 (2008) 34–45

Journal of Non-Newtonian Fluid Mechanics

www.elsevier.com/locate/jnnfm

An adaptive remeshing strategy for viscoelastic fluid flow simulations

R. Guénette [a], A. Fortin [a,*], A. Kane [a], J.-F. Hétu [a]

[a] GIREF, Département de mathématiques et de statistique, Université Laval, Québec, Canada G1K 7P4
[b] Institut des matériaux industriels, Conseil national de recherches du Canada, 75 boul. de Mortagne, Boucherville, Canada J4B 6Y4

Received 15 August 2007; received in revised form 21 November 2007; accepted 22 November 2007

Abstract

In the last few years, we have developed a fairly general adaptive finite element solution procedure which can be applied to a large variety of problems. In this paper, this strategy is briefly recalled and applied to the solution of two-dimensional viscoelastic fluid flow problems. A log-conformation formulation recently introduced by Fattal and Kupferman [R. Fattal, R. Kupferman, Time-dependent simulation of viscoelastic flows at high Weissenberg number using the log-conformation representation, J. Non-Newtonian Fluid Mech. 126 (2005) 23-37] was implemented in order to improve the convergence properties of the numerical scheme. We confirm some results obtained in Hulsen, Fattal and Kupferman [M. Hulsen, R. Fattal, R. Kupferman, Flow of viscoelastic fluids past a cylinder at high Weissenberg number: stabilized simulations using matrix logarithm, J. Non-Newtonian Fluid Mech. 127 (2005) 27-39] and in some instances, we show that mesh adaptation allows to almost automatically reproduce accurate results obtained on very fine structured meshes.

Keywords: Viscoelastic fluids; High Weissenberg problem; Log-conformation formulation; Error estimation; Adaptive remeshing; Finite element method

1. Introduction

The simulation of highly viscoelastic fluid flow problems is still plagued with the so-called high Weissenberg problem (HWP). The Weissenberg number *We* is the ratio of the magnitude of the elastic forces to that of the viscous forces. Most (if not all) numerical methods lose convergence i.e. fail to generate any result and/or fail to generate convergent solutions with respect to mesh size, at small or moderate Weissenberg numbers, limiting their use in industrial flow situations.

The source of the problem is partly numeric and partly due to questionable models such as Maxwell or Oldroyd. From a numerical standpoint, definite improvements were made possible by the introduction of more sophisticated numerical techniques: consistent discretisation of the different variables as in Fortin, Guénette and Pierre [3], Marchal and Crochet [4], etc; upwinding techniques for convective equations such as discontinuous Galerkin (see Fortin and Fortin [5]), SU and SUPG methods (see Crochet [4]); the introduction of more appropriate variational formulations such as the Elastic-Viscous Stress splitting (EVSS) of Rajagopalan et al. [6], etc.

Recently, a log-conformation formulation was proposed by Fattal and Kupferman [1] and further implemented in Hulsen, Fattal and Kupferman [2]. The main idea is to formulate the constitutive equation in term of the conformation tensor instead of the extra-stress tensor. More precisely, the constitutive equation is written in terms of the logarithm of the positive definite conformation tensor which is therefore well defined. This idea is new for viscoelastic fluid flow problems but was already used for the simulation of turbulent flow problems where the κ–ϵ model is frequently rewritten in terms of the variables $\mathcal{K} = \log\kappa$ and $\mathcal{E} = \log\epsilon$ as in Ilinca, Hétu and Pelletier [7]. One of the advantages is that when recovering $\kappa = \exp(\mathcal{K})$ or $\epsilon = \exp(\mathcal{E})$, the result is always positive which is not always the case with formulations using κ and ϵ directly. This formulation has also some good influence on the convergence properties of the numerical solver. Indeed, the logarithm of a variable presenting very steep variations is much easier to capture with a finite element discretisation.

Adaptive methods are now used extensively in CFD codes. Starting from a numerical solution, the error is estimated and the mesh is modified so that the numerical solution respects some prescribed error level. In particular, the development of anisotropic meshes where elements can present very large aspect ratios has received a lot of attention in the last few years. Robust anisotropic adaptive strategies require reliable and consistently

* Corresponding author.
E-mail address: afortin@giref.ulaval.ca (A. Fortin).

0377-0257/$ – see front matter © 2007 Elsevier B.V. All rights reserved.
doi:10.1016/j.jnnfm.2007.11.009

accurate solvers capable of dealing with strongly elongated elements appearing in unstructured meshes. This kind of solver was certainly not available for viscoelastic flows until recently. We believe that the introduction of the log-conformation tensor formulation is a huge step in the right direction. As shall be seen, using this formulation, it is now possible to compute complex viscoelastic flows, adapt the mesh and recompute a more accurate solution, often with fewer elements.

2. Governing equations

Let us consider the flow of a viscoelastic fluid in a spatial region Ω, having boundary Γ. The governing equations are the following:

Conservation of mass:

$$\nabla \cdot \boldsymbol{u} = 0 \tag{1}$$

Conservation of momentum for creeping flow:

$$-\nabla \cdot \boldsymbol{\tau} - \nabla \cdot (2\eta_{\mathrm{s}}\dot{\gamma}(\boldsymbol{u})) + \nabla p = 0 \tag{2}$$

In the above equations, p is the pressure, $\boldsymbol{u}$ is the velocity vector, $\dot{\gamma}(\boldsymbol{u})$ is the rate of deformation tensor:

$$\dot{\gamma}(\boldsymbol{u}) = \frac{\nabla \boldsymbol{u} + (\nabla \boldsymbol{u})^{\mathrm{t}}}{2} = \frac{\boldsymbol{L} + \boldsymbol{L}^{\mathrm{t}}}{2} \quad (\text{with } \boldsymbol{L} = \nabla \boldsymbol{u})$$

η_s is the solvent viscosity and $\boldsymbol{\tau}$ is the extra-stress tensor. The polymer contribution can be modeled by various constitutive equations. Two popular choices are the exponential Phan-Thien-Tanner model [8]:

$$\lambda \left(\frac{\partial \boldsymbol{\tau}}{\partial t} + \boldsymbol{u} \cdot \nabla \boldsymbol{\tau} - \boldsymbol{L} \cdot \boldsymbol{\tau} - \boldsymbol{\tau} \cdot \boldsymbol{L}^{\mathrm{t}} \right) + \exp\left(\frac{\lambda \epsilon}{\eta_{\mathrm{p}}} \mathrm{tr}(\boldsymbol{\tau}) \right) \boldsymbol{\tau} = 2\eta_{\mathrm{p}}\dot{\gamma}(\boldsymbol{u}) \tag{3}$$

and the Giesekus model:

$$\lambda \left(\frac{\partial \boldsymbol{\tau}}{\partial t} + \boldsymbol{u} \cdot \nabla \boldsymbol{\tau} - \boldsymbol{L} \cdot \boldsymbol{\tau} - \boldsymbol{\tau} \cdot \boldsymbol{L}^{\mathrm{t}} \right) + \boldsymbol{\tau} \left(\boldsymbol{I} + \frac{\alpha \lambda}{\eta_{\mathrm{p}}} \boldsymbol{\tau} \right) = 2\eta_{\mathrm{p}}\dot{\gamma}(\boldsymbol{u}) \tag{4}$$

In these constitutive equations, η_{p} is the viscosity of the polymer and λ a relaxation time. The parameter ϵ is a material constant related to the extensional viscosity. In both cases, the extra-stress tensor is related to the conformation tensor $\boldsymbol{c}$ by the relation:

$$\boldsymbol{\tau} = \frac{\eta_{\mathrm{p}}}{\lambda}(\boldsymbol{c} - \boldsymbol{I}) \tag{5}$$

Replacing in Eqs. (3) and (4), one can obtain a unique expression of the evolution equation of the conformation tensor that takes the following form:

$$\frac{\partial \boldsymbol{c}}{\partial t} + \boldsymbol{u} \cdot \nabla \boldsymbol{c} - \boldsymbol{L} \cdot \boldsymbol{c} - \boldsymbol{c} \cdot \boldsymbol{L}^{\mathrm{t}} = \boldsymbol{f}(\boldsymbol{c}) \tag{6}$$

with:

$$\boldsymbol{f}(\boldsymbol{c}) = \begin{cases} -\dfrac{\exp(\epsilon(\mathrm{tr}(\boldsymbol{c}) - 3))}{\lambda}(\boldsymbol{c} - \boldsymbol{I}) & (\text{PTT}) \\ -\left(\dfrac{\boldsymbol{I} + \alpha(\boldsymbol{c} - \boldsymbol{I})}{\lambda} \right)(\boldsymbol{c} - \boldsymbol{I}) & (\text{Giesekus}) \end{cases} \tag{7}$$

3. Log-conformation form of the constitutive equation

The log-conformation formulation has been introduced by Fattal and Kupferman [1] and further implemented by Hulsen, Fattal and Kupferman [1,2]. This new formulation appears as a promising approach to overcome the high Weissenberg number problem for viscoelastic fluid flow simulations.

In this section, we briefly recall the derivation of the log-conformation formulation. The details can be found in references [1,2]. Since the conformation tensor $\boldsymbol{c}$ is symmetric and positive definite (SPD), it takes the form:

$$\boldsymbol{c} = \boldsymbol{R} \cdot \boldsymbol{\Lambda} \cdot \boldsymbol{R}^{\mathrm{t}} \tag{8}$$

where $\boldsymbol{R}$ is an orthogonal tensor ($\boldsymbol{R} \cdot \boldsymbol{R}^{\mathrm{t}} = \boldsymbol{I}$) and $\boldsymbol{\Lambda}$ is a diagonal tensor containing the strictly positive eigenvalues λ_i of $\boldsymbol{c}$. The logarithm of the tensor $\boldsymbol{c}$ is then well defined as:

$$\boldsymbol{s} = \log \boldsymbol{c} = \boldsymbol{R} \cdot \log \boldsymbol{\Lambda} \cdot \boldsymbol{R}^{\mathrm{t}}$$

with $\log \boldsymbol{\Lambda}$ a diagonal matrix whose entries are $\log \lambda_i$.

Denoting $\boldsymbol{\Omega}$ the antisymmetric matrix $-\boldsymbol{R} \cdot \dot{\boldsymbol{R}}^{\mathrm{t}}$, where $\dot{\boldsymbol{R}}$ stands for the material derivative of $\boldsymbol{R}$, the constitutive Eq. (6) can be written along the principal axes of $\boldsymbol{c}$:

$$\tilde{\boldsymbol{\Omega}} \cdot \boldsymbol{\Lambda} + \boldsymbol{\Lambda} \cdot \tilde{\boldsymbol{\Omega}}^{\mathrm{t}} + \dot{\boldsymbol{\Lambda}} = (\tilde{\boldsymbol{L}} \cdot \boldsymbol{\Lambda} + \boldsymbol{\Lambda} \cdot \tilde{\boldsymbol{L}}^{\mathrm{t}}) + \boldsymbol{f}(\boldsymbol{\Lambda}) \tag{9}$$

In the above equation, the tensor $\boldsymbol{f}(\boldsymbol{\Lambda})$ is diagonal with entries $f_i(\lambda_1, \lambda_2, \lambda_3)$. The tensors $\tilde{\boldsymbol{\Omega}}$, $\tilde{\boldsymbol{L}}$ are related to $\boldsymbol{\Omega}$ and $\boldsymbol{L}$ by the relations $\boldsymbol{\Omega} = \boldsymbol{R} \cdot \tilde{\boldsymbol{\Omega}} \cdot \boldsymbol{R}^{\mathrm{t}}$ and $\boldsymbol{L} = \boldsymbol{R} \cdot \tilde{\boldsymbol{L}} \cdot \boldsymbol{R}^{\mathrm{t}}$. The constitutive Eq. (6) can then be expressed in terms of the logarithm of $\boldsymbol{c}$ which is the basic log-conformation form of Eq. (6):

$$\frac{\partial \boldsymbol{s}}{\partial \boldsymbol{t}} + \boldsymbol{u} \cdot \nabla \boldsymbol{s} - \boldsymbol{R} \cdot \left(\dot{\boldsymbol{\Lambda}} \cdot \boldsymbol{\Lambda}^{-1} + \tilde{\boldsymbol{\Omega}} \cdot \log \boldsymbol{\Lambda} + \log \boldsymbol{\Lambda} \cdot \tilde{\boldsymbol{\Omega}}^{\mathrm{t}} \right) \cdot \boldsymbol{R}^{\mathrm{t}} = 0 \tag{10}$$

Eq. (10) is still difficult to handle due to the presence of the matrices $\dot{\boldsymbol{\Lambda}} \cdot \boldsymbol{\Lambda}^{-1}$ and $\tilde{\boldsymbol{\Omega}} \cdot \log \boldsymbol{\Lambda} + \log \boldsymbol{\Lambda} \cdot \tilde{\boldsymbol{\Omega}}^{\mathrm{t}}$ that cannot be evaluated directly. On the one hand, $\dot{\boldsymbol{\Lambda}} \cdot \boldsymbol{\Lambda}^{-1}$ is diagonal and it is easy to show that:

$$\dot{\lambda}_i \lambda_i^{-1} = 2\tilde{L}_{ii} + \frac{f_i(\lambda_1, \lambda_2, \lambda_3)}{\lambda_i} \tag{11}$$

On the other hand, the matrix $\tilde{\boldsymbol{\Omega}} \cdot \log \boldsymbol{\Lambda} + \log \boldsymbol{\Lambda} \cdot \tilde{\boldsymbol{\Omega}}^{\mathrm{t}}$ is symmetric with zero diagonal entries and it can be shown that its off-diagonal terms are (for $i \neq j$):

$$\tilde{w}_{ij}(\log \lambda_j - \log \lambda_i) = \left(\frac{\log \lambda_j - \log \lambda_i}{\lambda_j - \lambda_i} \right)(\lambda_i \tilde{L}_{ji} + \lambda_j \tilde{L}_{ij}) \tag{12}$$

When $\lambda_j \neq \lambda_i$, this last expression is used. However, when $\lambda_j = \lambda_i$, a passage to the limit is necessary and we get:

$$\tilde{w}_{ij}(\log \lambda_j - \log \lambda_i) = (\tilde{L}_{ij} + \tilde{L}_{ji}) \tag{13}$$

In practice, the condition $|\lambda_j - \lambda_i| < \epsilon$ with ϵ of the order 10^{-8} is applied in order to switch between the two cases. Different values of ϵ has been tested with no significant changes.

4. Numerical discretisation

A finite element method is used for the spatial discretisation of this system of equations. In order to obtain a proper mixed finite element formulation, a Discrete Elastic–Viscous Split Stress (DEVSS) formulation introduced in Fortin, Fortin, Guénette and Pierre [9,3] is used for the discretizations of the momentum and the continuity equations as follows:

$$\begin{cases} -\nabla\cdot\boldsymbol{\tau} + \nabla\cdot(2\alpha\boldsymbol{d}) - \nabla\cdot(2(\eta_s+\alpha)\dot{\gamma}(\boldsymbol{u})) + \nabla p = 0 \\ \boldsymbol{d} - \dot{\gamma}(\boldsymbol{u}) = 0 \\ \nabla\cdot\boldsymbol{u} = 0 \\ \dfrac{\partial \boldsymbol{s}}{\partial \boldsymbol{t}} + \boldsymbol{u}\cdot\nabla\boldsymbol{s} - \boldsymbol{R}\cdot\left(\dot{\boldsymbol{\Lambda}}\cdot\boldsymbol{\Lambda}^{-1} + \tilde{\boldsymbol{\Omega}}\cdot\log\Lambda + \log\Lambda\cdot\tilde{\boldsymbol{\Omega}}^{\mathrm{t}}\right)\cdot\boldsymbol{R}^{\mathrm{t}} = 0 \\ \boldsymbol{\tau} - \dfrac{\eta_{\mathrm{p}}}{\lambda}(\exp\boldsymbol{s} - \boldsymbol{I}) = 0 \end{cases} \tag{14}$$

In this paper, the velocity is approximated by continuous quadratic polynomials, the pressure by continuous linear polynomials (the Taylor–Hood P_2–P_1 element). The logarithm of the conformation tensor ($\boldsymbol{s}$), the extra-stress ($\boldsymbol{\tau}$) and the rate of deformation ($\boldsymbol{d}$) have all been approximated by continuous linear polynomials. Denoting by $\boldsymbol{v}$, q, $\boldsymbol{\phi}_d$, $\boldsymbol{\phi}_s$ and $\boldsymbol{\phi}_\tau$ the weighting functions for the variables $\boldsymbol{u}$, p, $\boldsymbol{d}$, $\boldsymbol{s}$ and $\boldsymbol{\tau}$ respectively, the finite element system takes the form:

$$\begin{cases} \displaystyle\int_\Omega [-(\nabla\cdot\boldsymbol{\tau})\cdot\boldsymbol{v} - 2\alpha\boldsymbol{d} : \dot{\gamma}(\boldsymbol{v})\mathrm{d}x \\ \qquad +2(\eta_s+\alpha)\dot{\gamma}(\boldsymbol{u}) : \dot{\gamma}(\boldsymbol{v}) - p\nabla\cdot\boldsymbol{v}]\mathrm{d}x = 0 \\ \displaystyle\int_\Omega \nabla\cdot\boldsymbol{u}q\,\mathrm{d}x = 0 \\ \displaystyle\int_\Omega [\boldsymbol{d} - \dot{\gamma}(\boldsymbol{u})] : \boldsymbol{\phi}_d\mathrm{d}x = 0 \\ \displaystyle\int_\Omega \left[\frac{\partial \boldsymbol{s}}{\partial t} + \boldsymbol{u}\cdot\nabla\boldsymbol{s} - \boldsymbol{R}\cdot(\dot{\boldsymbol{\Lambda}}\cdot\boldsymbol{\Lambda}^{-1}\right. \\ \qquad \left. +\tilde{\boldsymbol{\Omega}}\cdot\log\boldsymbol{\Lambda} + \log\boldsymbol{\Lambda}\cdot\tilde{\boldsymbol{\Omega}}^{\mathrm{t}})\cdot\boldsymbol{R}^{\mathrm{t}}\right] : \boldsymbol{\phi}_s\mathrm{d}x = 0 \\ \displaystyle\int_\Omega \left[\boldsymbol{\tau} - \frac{\eta_{\mathrm{p}}}{\lambda}(\exp\boldsymbol{s} - \boldsymbol{I})\right] : \boldsymbol{\phi}_\tau\mathrm{d}x = 0 \end{cases} \tag{15}$$

An implicit Euler scheme is used to discretise the time derivative, hence $\partial\boldsymbol{s}/\partial t \approx \boldsymbol{s}^{n+1} - \boldsymbol{s}^n/\Delta t$ and all other terms are evaluated at time $\boldsymbol{t}_{n+1}$. Eq. (10) is hyperbolic and a streamline upwind Petrov–Galerkin (SUPG) was used. It consists in replacing the weighting functions $\boldsymbol{\phi}_s$ by $\boldsymbol{\phi}_s + \alpha\boldsymbol{u}\cdot\nabla\boldsymbol{\phi}_s$ in every term of the system (15). In the above expression, $\alpha = h/U$ with h a characteristic length-scale of the element and U is a characteristic velocity.

The non-linearity of the constitutive equation requires a Newton method to achieve convergence. It is however quite difficult to linearise this equation in a standard manner. For this reason, the Jacobian matrix was approximated using finite differences. Consequently, it is only necessary to be able compute the equation residual for a given value of $\boldsymbol{s}$. This residual (see the second to last equation in system (15)) can be computed as follows:

(1) $\boldsymbol{s}$ is first decomposed into $\boldsymbol{R}\cdot\log\boldsymbol{\Lambda}\cdot\boldsymbol{R}^{\mathrm{t}}$;
(2) the eigenvalues λ_i are computed by taking the exponential of the eigenvalues of $\boldsymbol{s}$;
(3) $\tilde{\boldsymbol{L}}$ is the evaluated using $\tilde{\boldsymbol{L}} = \boldsymbol{R}^{\mathrm{t}}\cdot\boldsymbol{L}\cdot\boldsymbol{R}$;
(4) matrix $\dot{\boldsymbol{\Lambda}}\cdot\boldsymbol{\Lambda}^{-1}$ is evaluated using (11);
(5) matrix $\tilde{\boldsymbol{\Omega}}\cdot\log\boldsymbol{\Lambda} + \log\boldsymbol{\Lambda}\cdot\tilde{\boldsymbol{\Omega}}^{\mathrm{t}}$ is evaluated using (12) if $\lambda_i \neq \lambda_j$ and using (13) if $\lambda_i = \lambda_j$;

The complete solution procedure is the following:
At each time step;

(1) Solve for ($\boldsymbol{u}$, p), $\boldsymbol{\tau}$, $\boldsymbol{d}$ being known;
(2) Solve for $\boldsymbol{d}$, which is an L^2-projection of $\dot{\gamma}(\boldsymbol{u})$;
(3) Solve for $\boldsymbol{s}$ using the velocity field calculated in step (1).
(4) Solve for $\boldsymbol{\tau}$, which is also an L^2-projection.

For a given time step, the above steps are performed iteratively until all variables are converged.

5. Anisotropic mesh adaptation

Adaptive remeshing strategies are now commonly used in CFD codes since they allow to control the error level on a given numerical solution thus providing very accurate solutions. The idea is simple: a first mesh is provided, the corresponding solution is computed and the error is estimated using some *a posteriori* error estimator. The mesh is then modified accordingly and a new solution is computed. The process is repeated many times until the numerical solution and the mesh no longer change and/or some error level has been reached. One of the basic ingredients for a successful adaptive method is a solver capable to provide a numerical solution on various unstructured meshes with possibly severe refinement in some regions of the computational domain. This was not possible for viscoelastic fluids until very recently due to convergence failure of most numerical codes on unstructured or very refined meshes (the high Weissenberg problem).

Adaptive remeshing strategies allow the concentration of small elements only where needed, that is where the error is estimated large. Moreover, our adaptive method allows for anisotropic meshes where some elements can be stretched in some preferential directions. Some elements can thus present very large aspect ratio. The most important consequence is the reduction of the number of elements needed to obtain an accurate solution. In finite element textbooks, elongated elements are often believed to give poor numerical solutions. This is true only if they are stretched in inappropriate directions. For example, in CFD computations, it would be ill advised to position an element stretched perpendicularly across a shock. But if the same element is reoriented tangentially, then the numerical solution can be very accurate.

The anisotropic adaptive strategy used in this work was introduced in Fortin, Belhamadia and Chamberland [10,11] for phase change problems in cryotherapy. It was also used in [12,13] for drop deformation in two and three dimensions. The methodology will not be recalled here and the reader is referred to these papers for a more complete description. The mesh adaptation strategy is general and can be used for all sorts of problems.

Based on our experience, among all the variables of the problem ($\boldsymbol{u}$, p, $\boldsymbol{c}$, $\boldsymbol{\tau}$ and $\boldsymbol{d}$), $\boldsymbol{\tau}$ is most sensitive and the use the Frobenius norm of $\boldsymbol{\tau}$ ($|\boldsymbol{\tau}| = \sqrt{\sum_{ij}\tau_{ij}\tau_{ij}}$) is adequate to drive the mesh adaptation process. Denoting $E_{|\tau|}$ the estimated absolute error on $|\boldsymbol{\tau}|$, the mesh is adapted until the estimated relative error (in L^2-norm) reaches a prescribed value e_p:

$$\frac{||E_{|\tau|}||_{0,\Omega}}{||\boldsymbol{\tau}||_{0,\Omega}} = \left(\frac{\int_\Omega E_{|\tau|}^2 \mathrm{d}x}{\int_\Omega |\boldsymbol{\tau}|^2 \mathrm{d}x}\right)^{1/2} = e_\mathrm{p}$$

The value of e_p was set to approximately 2% in the numerical results.

To control the error, a reinterpolation error estimator was used. The technique essentially relies on the assumption that a reasonable estimate of the error can be obtained from a suitable reinterpolation of the numerical solution (or in this case of $|\boldsymbol{\tau}|$). Starting from a standard C^0 (Lagrange) finite element solution u_h of degree k, an approximation of the first and second order derivatives at the vertices of the triangulation is needed. Since u_h is not differentiable, this is accomplished by solving a least square problem on a patch of elements adjacent to the given vertex. Once the derivatives have been computed, a Hermite finite element reinterpolation of the numerical solution is constructed. The error is then estimated as the difference between this Hermite reinterpolation and the initial (Lagrange) numerical solution.

Once the error has been estimated, the mesh is modified using local operations on the mesh:

- edge refinement;
- edge swapping;
- vertex suppression;
- vertex displacement.

The reader is referred once again to [10] for a complete description. As shall be seen, these local operations are sufficient to produce anisotropic meshes when needed.

To summarise, the main steps of the adaptive procedure are the following:

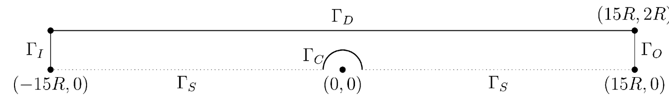

Fig. 1. Flow around a circular cylinder of radius R

- An initial mesh is provided and system (15) is solved;
- The error in the Frobenius norm of $\boldsymbol{\tau}$ is estimated;
- The mesh is then modified using local operations. Nodes and edges are swept a few times in order to perform:
  - ◦ Edge refinement and node suppression to control the error level;
  - ◦ Edge swapping, and node displacement to control the quality of the elements;
- ◦ A new mesh is produced and the process is repeated until the desired error level is reached.

6. Results and discussions

We consider the planar flow of a viscoelastic fluid around a circular cylinder of radius R centered at the origin. The cylinder is placed between two parallel plates separated by a distance $2H$. The ratio H/R is equal to 2 and the total length of the computational domain is 30 $R = 15H$. Symmetry considerations allow to make the computation in a half geometry. The computational domain Ω is presented in Fig. 1.

The flow around a circular cylinder using the Oldroyd-B model is known as a difficult problem where many if not all numerical methods fail to converge past a Weissenberg number around 1 i.e. either fail to give any results or the obtained numerical solutions do not converge with mesh size. This problem has however, received a lot of attention and is therefore an interesting (and difficult) benchmark.

Various numerical methods have been employed to solve this problem. Étienne et al. [14] used a Lagrangian-Eulerian approach, while Owens et al. [15] preferred a spectral method combined with a SUPG method. Fan et al. [16] used a Galerkin/least-square approach combined with a h–p finite element method to produce very accurate solutions. Their results were later confirmed by Alves et al. [17] with a finite volume method on very fine meshes. We will also compare our results with those of Hulsen et al. [2] who used a discontinuous Galerkin method.

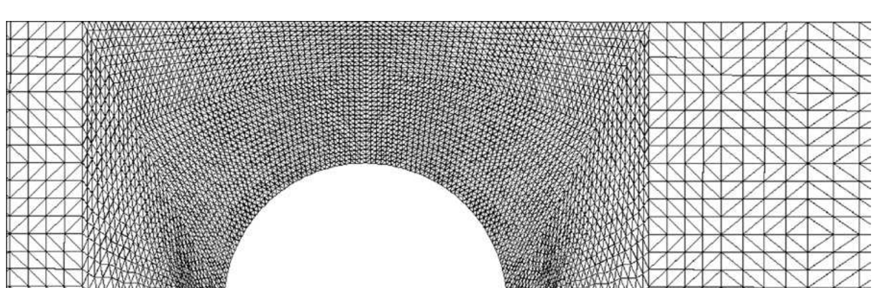

Fig. 2. Partial view of the structured mesh (9760 elements)

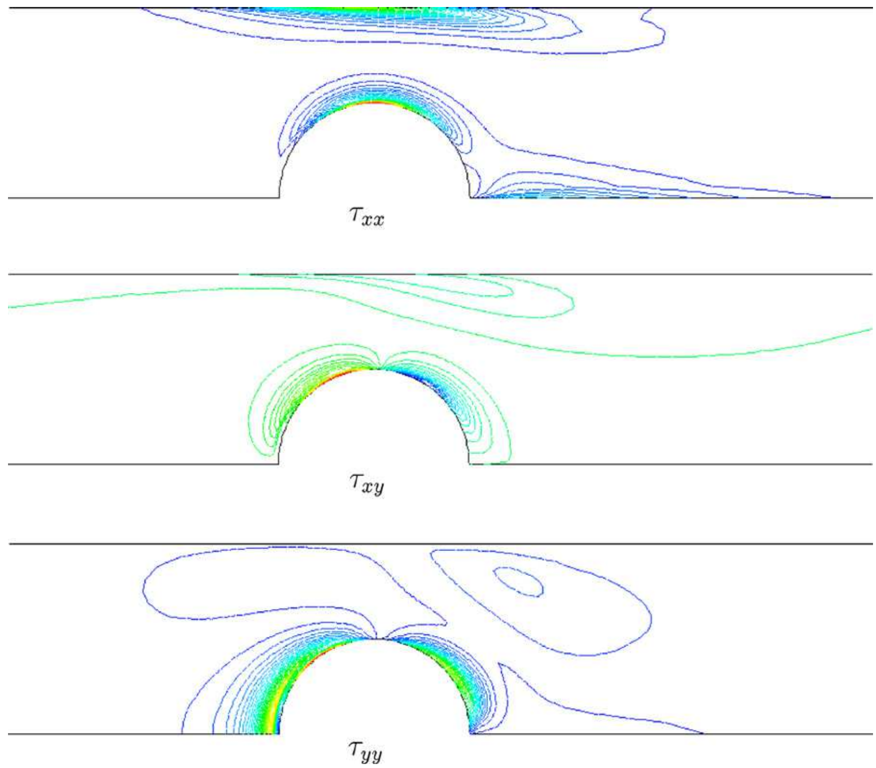

Fig. 3. Extra-stress components at $We = 0.8$ on the structured mesh (Oldroyd-B)

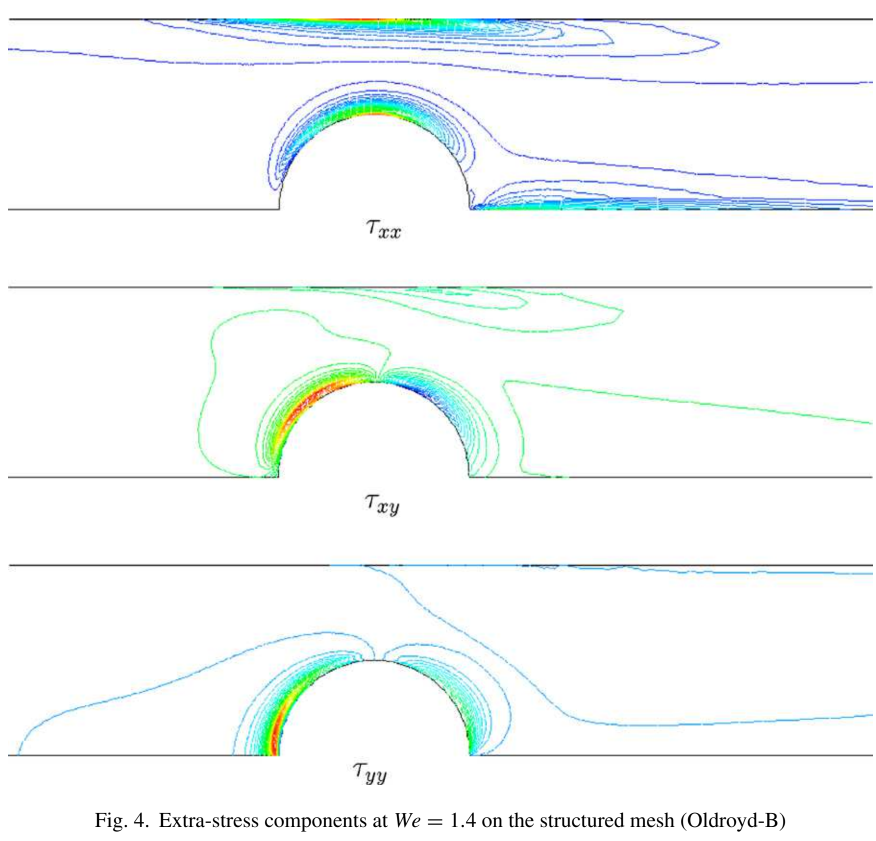

Fig. 4. Extra-stress components at $We = 1.4$ on the structured mesh (Oldroyd-B)

6.1. Numerical results (Oldroyd-B model)

As already mentioned, the Oldroyd B model can be recovered from the PTT model by setting $a = 0$ and $\epsilon = 0$. For comparison purposes with existing numerical results, we have chosen the following dimensionless parameters: $\eta_p = 0.41$ and $\eta_s = 0.59$. The Weissenberg number was defined as:

$$We = \frac{\lambda U}{R} \quad \text{with} \quad U = \frac{Q}{2H}$$

where U is the average velocity and Q is the flow rate.

The boundary conditions are as usual: no-slip ($\boldsymbol{u} = 0$) on the solid wall Γ_D and on the cylinder Γ_C; a symmetry condition $u_y = 0$ is imposed on the symmetry axis Γ_S; the flow far downstream from the cylinder is supposed to be fully developed and consequently, it is reasonable to impose $u_y = 0$ and the natural boundary condition $-p + 2\eta_s \partial u_x/\partial x = 0$. These two conditions are frequently employed for Newtonian fluids. For viscoelastic fluids, two possibilities exist depending if the term:

$$\int_\Omega -(\nabla \cdot \boldsymbol{\tau}) \cdot \boldsymbol{v} \mathrm{d}x \tag{16}$$

is integrated by parts or not. If (16) is integrated by parts, the natural exit condition would be to impose $-p + 2\eta_s \partial u_x/\partial x + \tau_{xx}$, which is generally unknown. For this reason, we did not integrate (16) by parts and our exit condition is valid on Γ_O.

At the inflow boundary Γ_I, the velocity is imposed as a fully established Poiseuille flow i.e.

$$u_x = \frac{3Q(H^2 - y^2)}{4H^3}, \quad u_y = 0$$

The tensor $\boldsymbol{s}$ must also be provided on the inlet boundary. For this purpose, the expression for $\boldsymbol{\tau}$ corresponding to a Poiseuille flow is first computed. From Eq. (5), the conformation tensor $\boldsymbol{c}$ can be obtained and decomposed into the form (8). From this, $\boldsymbol{s}$ can be easily computed. To avoid the imposition of inlet and outlet boundary conditions, periodic boundary conditions were used in [2] but this does not modify significantly the flow in the vicinity of the cylinder.

The drag around the cylinder was computed. This is obtained by computing:

$$(F_x, F_y) = \int_{\Gamma_C} \boldsymbol{\sigma} \cdot \boldsymbol{n} \mathrm{d}s$$

where $\boldsymbol{\sigma} = -p\boldsymbol{I} + 2\eta_s \dot{\gamma}(\boldsymbol{u}) + \boldsymbol{\tau}$ is the Cauchy stress tensor and $\boldsymbol{n}$ is the unit normal to the cylinder. This quantity is a two-dimensional vector whose vertical component F_y vanishes due to the symmetry of the problem. This boundary integral was computed using three Gauss points on each edge on the cylinder.

In the numerical results, we will only present dimensionless quantities: length has been made dimensionless using R, velocities using U and stresses using $(\eta_p + \eta_s)U/R$. Consequently, the dimensionless drag is defined as:

$$\tilde{F}_x = \frac{F_x}{(\eta_s + \eta_p)UR} = \frac{2HF_x}{(\eta_s + \eta_p)QR}$$

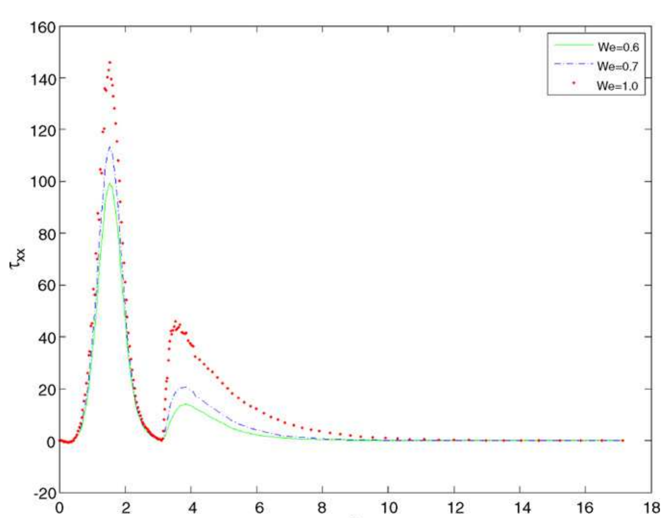

Fig. 5. τ_{xx} along the cylinder surface and in the wake on the structured mesh (Oldroyd-B)

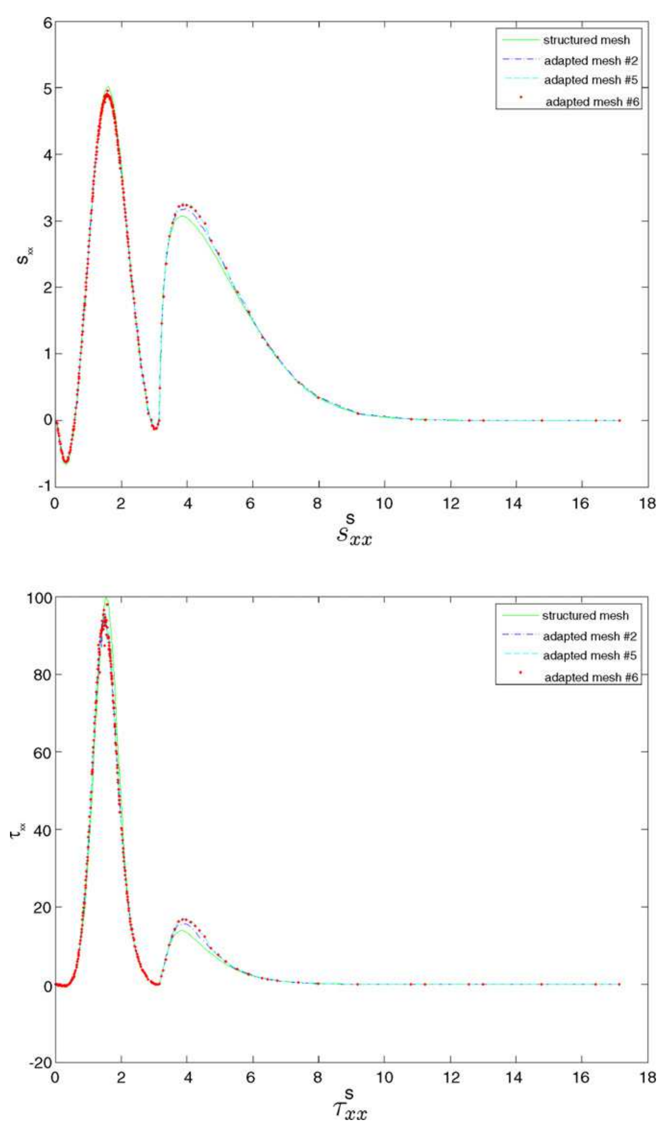

Fig. 6. Convergence with mesh size at $We = 0.6$ (Oldroyd-B)

Table 1
Dimensionless drag on structured mesh

We	Present work	Ref. [2]	Ref. [16]	Ref. [15]
0		132.358	132.36	132.357
0.1		130.363	130.36	
0.2	126.51	126.626	126.62	
0.4	120.48	120.596	120.59	
0.6	117.70	117.792	117.77	117.775
0.8	117.31	117.373	117.32	117.237
1.	118.35	118.501	118.49	118.030
1.2	120.82	120.650		119.764

Table 2
Adapted meshes at $We = 0.6$ using (Oldroyd-B)

Mesh	Number of elements
Mesh #1	9603
Mesh #2	8610
Mesh #3	7986
Mesh #4	7646
Mesh #5	7446
Mesh #6	7501

For the first computations, a 9760 elements structured mesh (see Fig. 2) similar to mesh M5 (7680 elements) in reference [2] was used. On this mesh, we were able to compute solutions up to $We = 1.7$. This is comparable to the limit observed in [2]. These solutions were computed on one mesh and no convergence analysis with mesh size was attempted.

Isocontours of the extra-stress tensor $\boldsymbol{\tau}$ are presented in Fig. 3 at $We = 0.8$ and in Fig. 4 at $We = 1.4$. The isocontours look very smooth and do not present spurious oscillations. Clearly, as the Weissenberg number increases, high stresses develop on the surface of the cylinder. The component τ_{xx} also presents high stresses on the symmetry axis behind the cylinder as can be seen in Fig. 5. These extreme values increase both on and in the wake of the cylinder as the Weissenberg number increases. This will have important consequences. Our results are in very good agreement with those of reference [2].

Our drag computations are presented in Table 1 and compared with those of references [2,15,16]. The observed differences are very small and could be easily explained by the meshes, the upwinding methods or the discretizations of the different variables used in these various references.

It was argued in [2] that despite the fact that it was possible to compute numerical solutions for Weissenberg numbers larger than 0.6, convergence with mesh size was not necessarily attainable. We have thus employed our adaptive strategy for the numerical solutions at $We = 0.6$, $We = 0.7$, and $We = 0.8$.

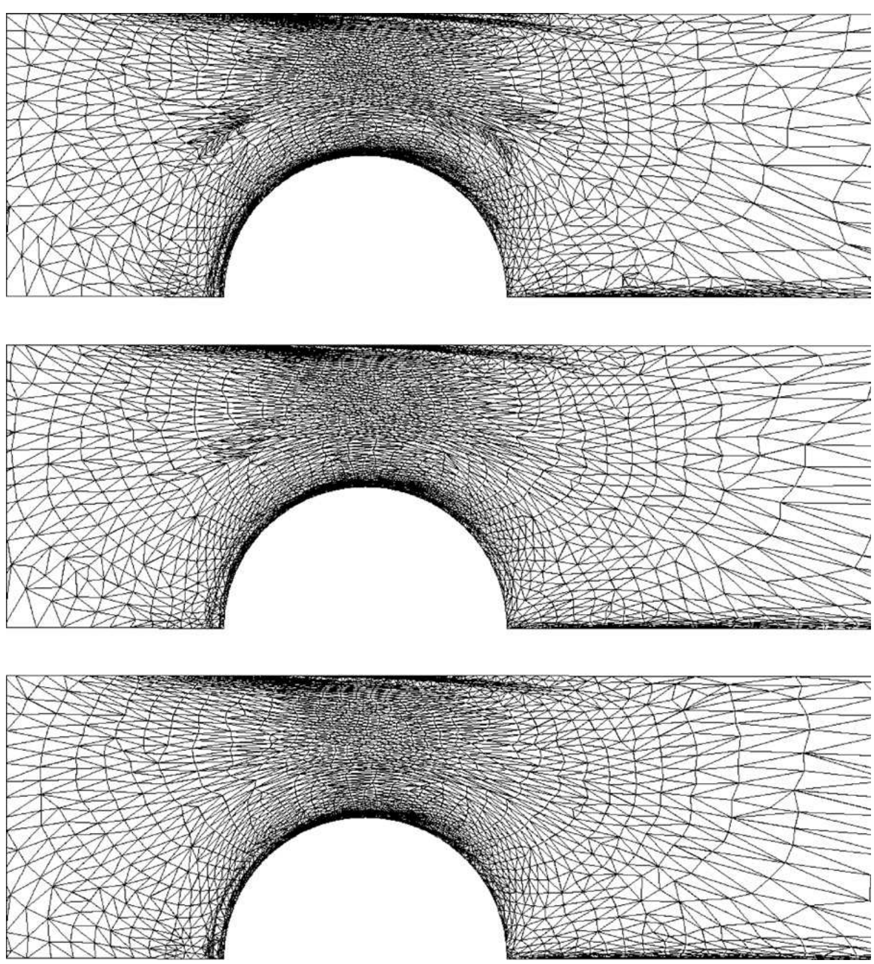

Fig. 7. Adapted meshes #2, #4 , #6 at $We = 0.7$.

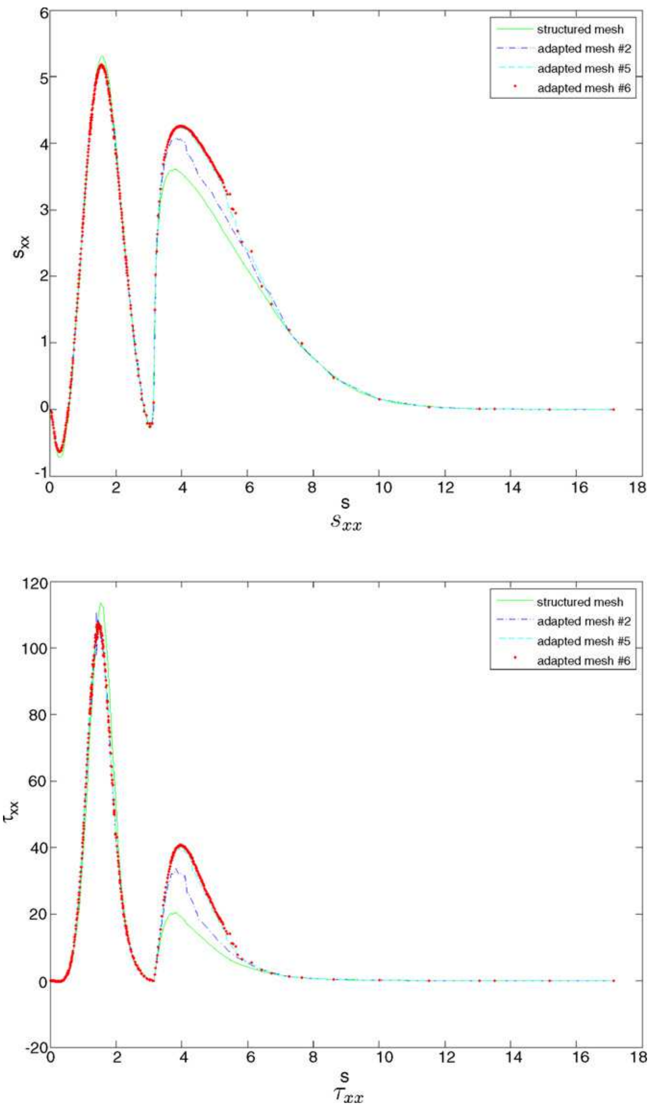

Fig. 8. Convergence with mesh size at $We = 0.7$ (Oldroyd-B)

At $We = 0.6$, a series of six meshes was obtained containing approximately 7500 elements (see Table 2 for the details). As the number of adaptations increases, the number of elements meshes seems to converge as can be seen from the Table 2. The different meshes present high element concentration on the cylinder. The computed log-conformation s_{xx} and the stress component τ_{xx} along the cylinder and on the symmetry axis are presented in Fig. 6. Results show a clear mesh convergence since the solutions no longer evolve with the adapted meshes. Here again, our results are in very good agreement with those of reference [2].

Table 3
Adapted meshes at $We = 0.7$ using (Oldroyd-B)

Mesh	Number of elements
Mesh #1	10156
Mesh #2	9621
Mesh #3	9848
Mesh #4	10379
Mesh #5	11027
Mesh #6	11563

Table 4
Adapted meshes at $We = 0.8$ using (Oldroyd-B)

Mesh	Number of elements
Mesh #1	12509
Mesh #2	13598
Mesh #3	17745

The situation at $We = 0.7$ has also been addressed in [2] where convergence with mesh size could not be reached nor demonstrated. Here again, six adapted meshes were obtained and the details are given in Table 3. The number of elements does not stabilize as neatly as for $We = 0.6$ but does not excessively increase either. Fig. 7 illustrates meshes #2, #4 and #6 where high concentrations of elements on the cylinder and on the symmetry axis in its wake can be seen. This is consistent with the results of Alves et al. [17] who suggested that wake-refined meshes are

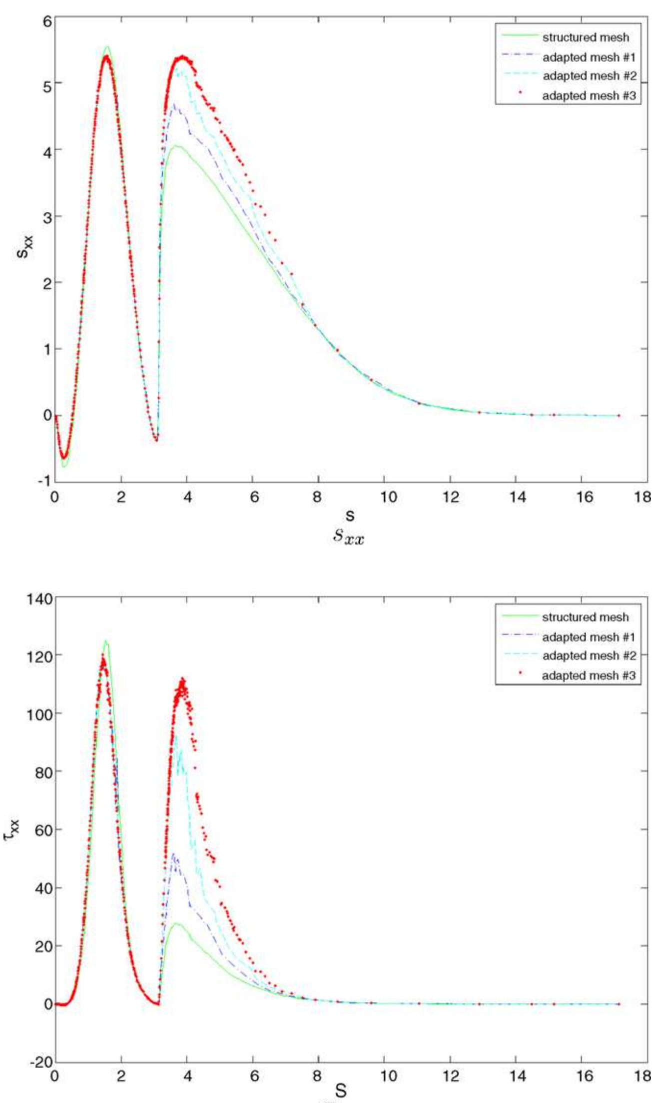

Fig. 9. Non convergence with mesh size at $We = 0.8$ (Oldroyd-B)

Table 5
Adapted meshes using at $We = 1$ (Giesekus)

Mesh	Number of elements
Mesh #1	7414
Mesh #2	6171
Mesh #3	7101
Mesh #4	7012
Mesh #5	7069
Mesh #6	7042

Table 6
Adapted meshes using at $We = 5$ (Giesekus)

Mesh	Number of elements
Mesh #1	9436
Mesh #2	10862
Mesh #3	11875
Mesh #4	11639
Mesh #5	11600
Mesh #6	11586

needed in order to reproduce highly accurate results such as those of Fan et al. [16] for the same Weissenberg number. This is a clear advantage of mesh adaptation since these important regions are automatically detected. The computed log-conformation s_{xx} and the stress component τ_{xx} along the cylinder and on the symmetry axis are presented in Fig. 8. Can we say that mesh convergence has been achieved? From Fig. 8, the solutions no longer change on the last two meshes. Moreover, our solutions are very close to those obtained by Alves et al. [17] and Fan et al. [16] on much finer discretizations. This seems to confirm the results of reference [2] who postulate that convergence with mesh size was still possible at $We = 0.7$, at least using the Oldroyd-B model. The fact that the number of elements does not stabilise as nicely as for $We = 0.6$ (see the Tables 2 and 3) seems to indicate that $We = 0.7$ is close to a limiting value for mesh convergence for the Oldroyd-B model.

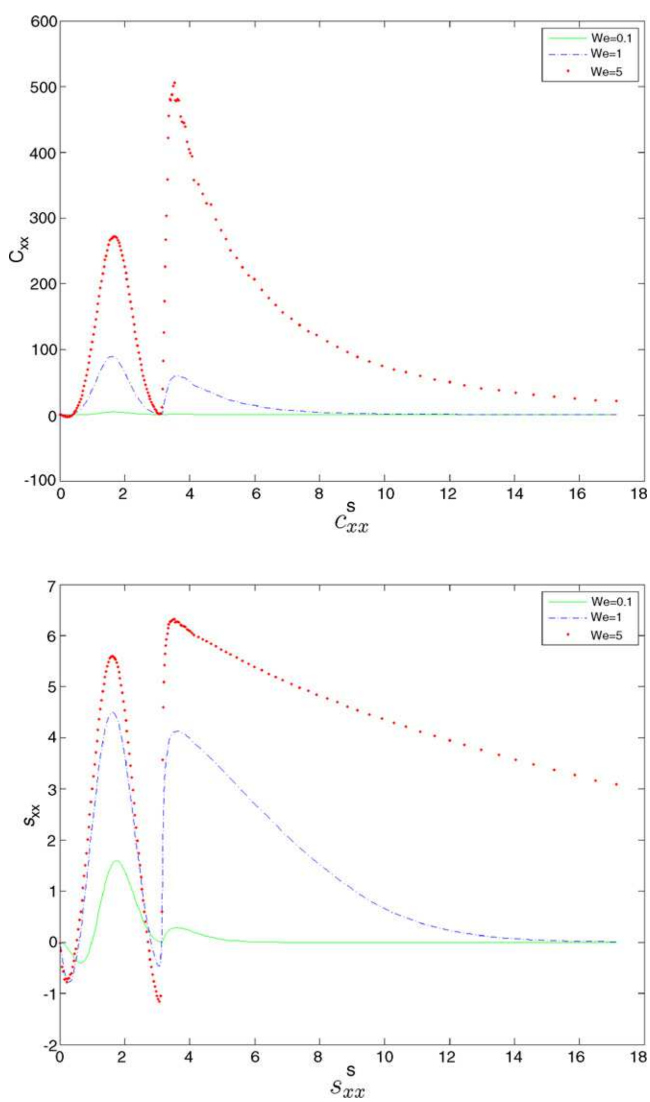

Fig. 10. c_{xx} and s_{xx} along the cylinder surface and in the wake on structured mesh (Giesekus)

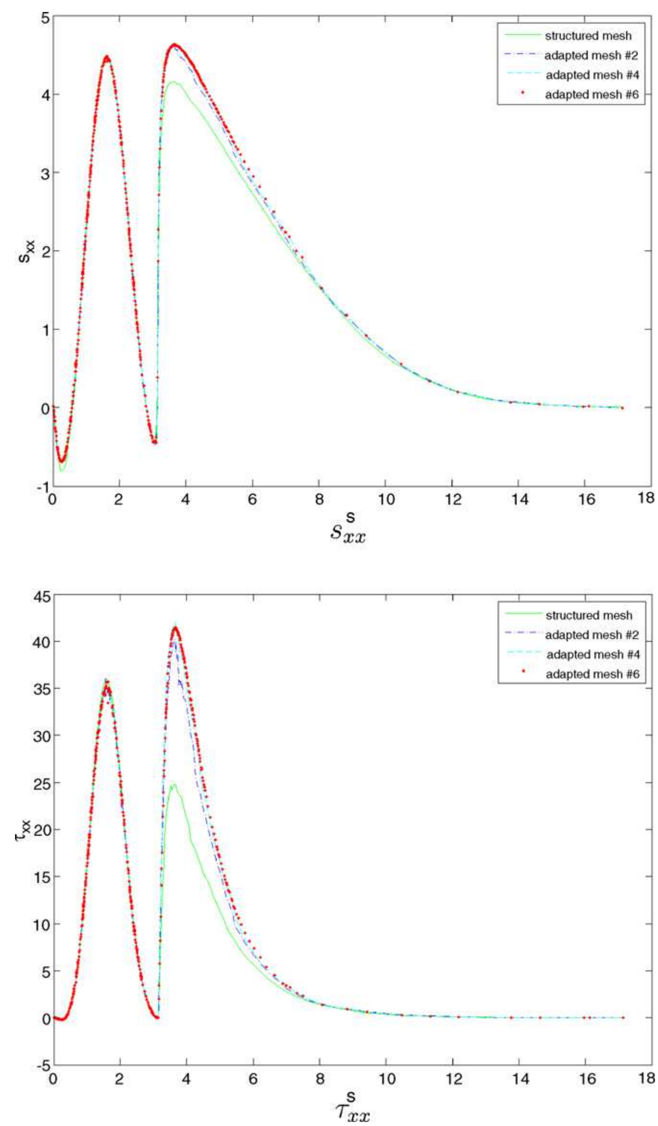

Fig. 11. s_{xx} and τ_{xx} along the cylinder surface and in the wake at $We = 1$. (Giesekus)

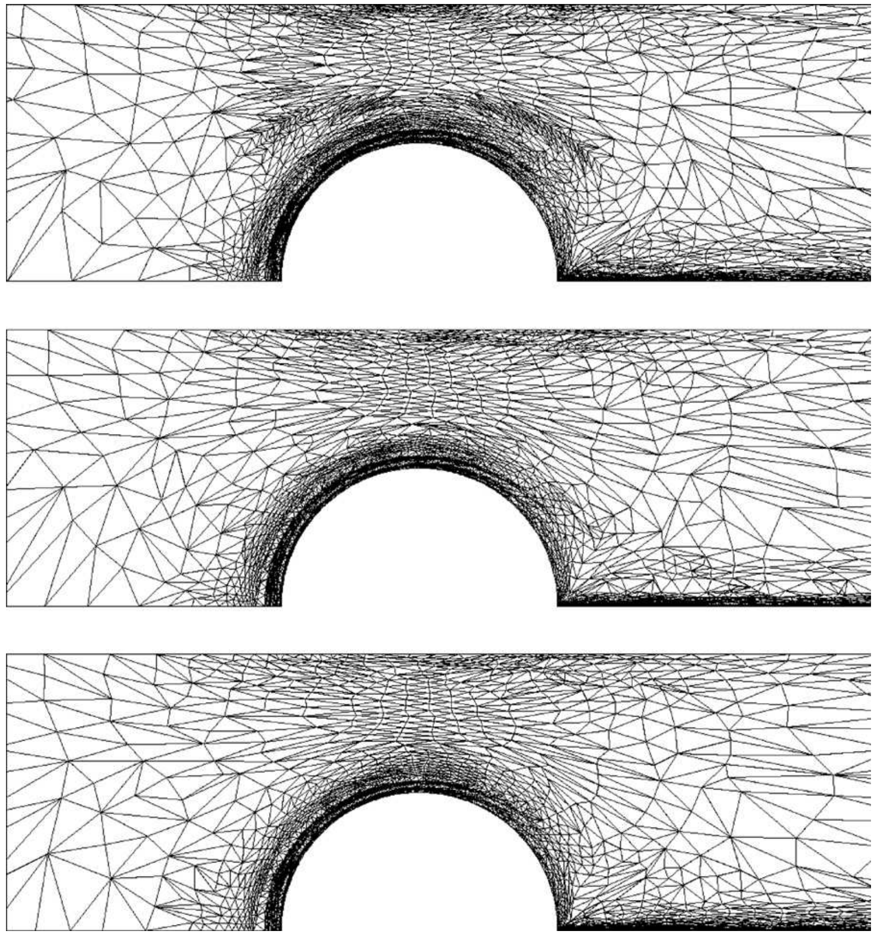

Fig. 12. Adapted meshes #2, #4 , #6 at $We = 5$. (Giesekus)

The situation is indeed entirely different at $We = 0.8$. A similar strategy was used with a series of adapted meshes (see Table 4). But differently from the previous cases, although the error level remains constant, we observed that the number of elements in the adapted meshes always increases. We have thus been forced to restrict the number of adaptations to three meshes. The computed stress component τ_{xx} along the cylinder and on the symmetry axis are presented in Fig. 9. The solutions are similar on the cylinder but the different solutions are extremely oscillatory on the symmetry axis behind the cylinder. The maximum value of the stresses also increases with each adaptation step. Very significant differences between the regular mesh and the adapted meshes are observed, indicating that convergence with mesh size has not be attained at $We = 0.8$. We have not tried to locate precisely the limiting Weissenberg number where convergence with mesh size fails.

6.2. Numerical results (Giesekus model)

In the following computations, the same values of η_p and η_s were used while α was set to 0.01 in the Giesekus model (4) as in [2]. The same boundary conditions as for the Oldroyd-B model were used.

The computations were first performed with the structured mesh of Fig. 2 and no limit Weissenberg number was found. The solution evolves smoothly with the Weissenberg number as shown in Fig. 10 where c_{xx} and the log matrix s_{xx} are illustrated on the cylinder and on the symmetry axis behind.

The question of mesh convergence was raised again. We first consider the solution at $We = 1$. Six meshes were obtained and Table 5 gives the number of elements for each mesh. This number quickly stabilises to around 7000 elements. The different solutions are presented in Fig. 11 where s_{xx} and τ_{xx} are traced. The solutions on the last meshes are indistinguishable. Hence, we consider that convergence with mesh size was attained.

In [2], convergence with mesh was not reached at $We = 5$ but they conjectured that with a sufficiently refined mesh, convergence could be achieved. Here again, six meshes were computed (see Table 6) and the number of elements stabilises around 11 500. Some of these meshes are presented in Fig. 12 where it is easily seen that the mesh adaptation procedure continues to put more and more elements on the cylinder surface and in its wake. The corresponding solutions are compared in Fig. 13. The different solution curves associated to the log matrix s_{xx} are almost superimposed except the one obtained on the structured mesh. A new solution feature seems to appear right at the end of the cylinder surface. Very steep variations of c_{xx} and s_{xx} are now present that were not observed for the Oldroyd-B model (at least at Weissenberg numbers smaller than 1). The mesh adaptation method does a very good job at refining the mesh in that region.

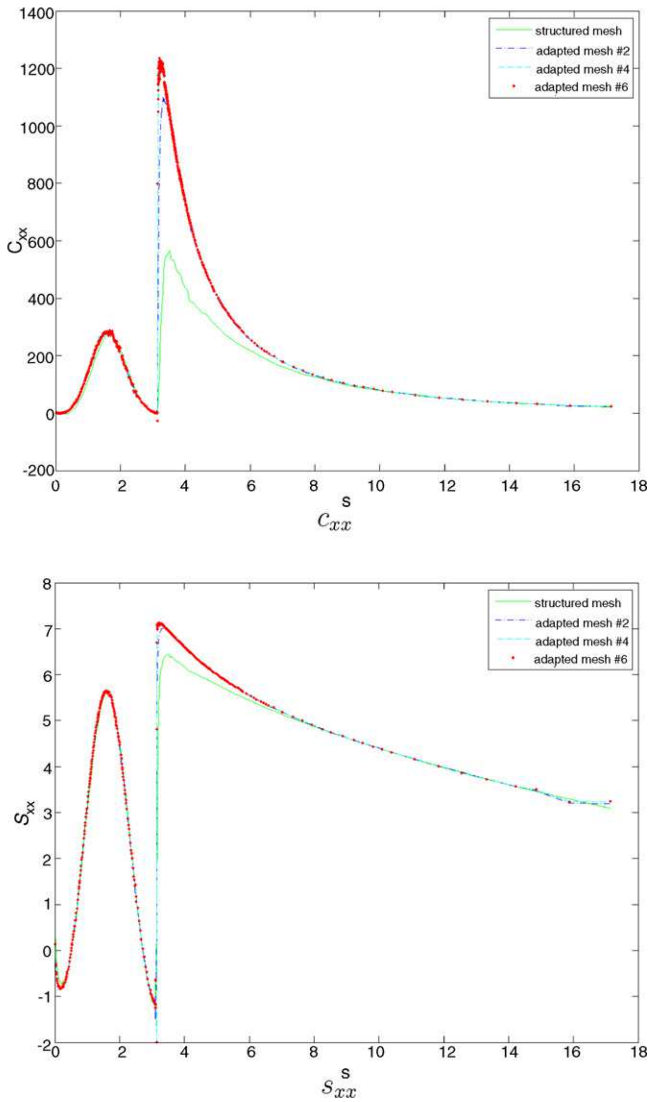

Fig. 13. c_{xx} and s_{xx} along the cylinder surface and in the wake at $We = 5$. (Giesekus)

Despite the very refined mesh, small amplitude oscillations are now present, barely seen on the variable c_{xx} but very clear on s_{xx} at this precise location. These oscillations could possibly be explained by the insufficient capability of the SUPG method to deal with sharp transitions in mesh size in that region. But here again, our results are in very good agreement with those of reference [2]. We therefore affirm that convergence with mesh size was achieved.

7. Conclusions

Computations have been performed for the simulation of the planar flow of a viscoelastic fluid around a cylinder using the Oldroyd-B and the Giesekus models. This problem is representative of all the difficulties plaguing the simulation of viscoelastic fluid flow at high Weissenberg numbers. In this work, a finite element method based on a log-conformation formulation was used. To further improve the accuracy of the simulations, an anisotropic adaptive remeshing method was introduced to study convergence with mesh size and to answer some of the questions raised in [2]. The log-conformation formulation allows the computation of numerical solutions on the highly unstructured meshes generated by our adaptive remeshing strategy. This kind of computations was hardly possible before.

By the introduction of an anisotropic adaptive remeshing strategy, we have shown that mesh convergence is possible for the Oldroyd-B model up to at least $We = 0.7$. We have been able to successfully reproduce the best numerical results found in the literature for the same problem. This Weissenberg number is apparently very close to the limiting value where convergence with mesh size can be achieved. This is also confirmed by our results at $We = 0.8$ where mesh convergence was lost.

For the Giesekus model however, the situation is different. We have been able to obtain convergence with mesh size up to at least $We = 5.0$, a result also conjectured in [2]. On structured meshes, there does not seem to exist a limiting Weissenberg number. This does not mean that convergence with mesh size is possible for all Weissenberg numbers. As the Weissenberg number increases, very steep variations of s_{xx} and c_{xx} appear right at the end of the cylinder. Our mesh adaptation method concentrates an increasingly large number of elements on the cylinder and in its wake in order to maintain the same level of accuracy on the numerical solution. The number of elements drastically increases (and therefore the computational burden) so that convergence with mesh size is more and more expensive and difficult. We do not believe that we will be able to reach convergence with mesh size at very high Weissenberg numbers. An efficient mesh adaptation procedure will definitely help but the number of elements will still make the computational cost extremely high if one wants to clearly establish convergence with mesh size. For this reason, we believe it is premature to say that the high Weissenberg problem is entirely behind us.

We, however, believe that the introduction of the log-conformation formulation of Fattal and Kupferman [1,2] represents a definite improvement over classical formulations. We are now capable of getting numbers out of the computer when performing numerical simulations on non-trivial problems. This does not mean at all that these numbers are valuable but at least, we are now in a position to study the solution behaviour on very fine and unstructured meshes. We can turn our attention towards more complex constitutive equations and more realistic problems.

Acknowledgements

The authors wish to acknowledge the financial support of the Natural Sciences and Engineering Research Council of Canada (NSERC).

References

[1] R. Fattal, R. Kupferman, Time-dependent simulation of viscoelastic flows at high Weissenberg number using the log-conformation representation, J. Non-Newtonian Fluid Mech. 126 (2005) 23–37.

[2] M. Hulsen, R. Fattal, R. Kupferman, Flow of viscoelastic fluids past a cylinder at high Weissenberg number: Stabilized simulations using matrix logarithm, J. Non-Newtonian Fluid Mech. 127 (2005) 27–39.

[3] A. Fortin, R. Guénette, R. Pierre, On the discrete EVSS method, Comput. Meth. Appl. Mech. Eng. 189 (1) (2000) 121–139.

[4] J.M. Marchal, M.J. Crochet, A new mixed finite element for calculating viscoelastic flows, J. Non-Newtonian Fluid Mech. 26 (1987) 77–114.

[5] M. Fortin, A. Fortin, A new approach for the FEM simulation of viscoelastic flows, J. Non-Newtonian Fluid Mech. 32 (1989) 295–310.

[6] D. Rajagopalan, R.A. Brown, R.C. Armstrong, Finite element methods for calculation of steady viscoelastic flow using constitutive equation with Newtonian viscosity, J. Non-Newtonian Fluid Mech. 36 (1990) 159–199.

[7] F. Ilinca, J.-F. Hétu, D. Pelletier, A unified finite element algorithm for two-equation models of turbulence, Comput. Fluid. 27 (3) (1998) 291–310.

[8] N. Phan Thien, R.I. Tanner, A new constitutive derived from network theory, J. Non-Newtonian Fluid Mech. 2 (1977) 353–365.

[9] M. Fortin, R. Guénette, R. Pierre, Numerical analysis of the modified EVSS method, Comput. Method. Appl. Mech. Eng. 143 (1997) 79–95.

[10] Y. Belhamadia, A. Fortin, É. Chamberland, Anisotropic mesh adaptation for the solution of the Stefan problem, J.Comput. Phys. 194 (1) (2004) 233–255.

[11] Y. Belhamadia, A. Fortin, É. Chamberland, Three-dimensional anisotropic mesh adaptation for phase change problems, J. Comput. Phys. 201 (2) (2004) 753–770.

[12] A. Fortin, K. Benmoussa, An adaptive remeshing strategy for free-surface fluid flow problems. Part I: the axisymmetric case., J. Polymer Eng. 26 (1) (2006) 21–58.

[13] K. Benmoussa, A. Fortin, An adaptive remeshing strategy for free-surface fluid flow problems. Part II: the three-dimensional case, J. Polymer Eng. 26 (1) (2006) 59–86.

[14] J. Étienne, E.J. Hinch, J. Li, A Lagrangian-Eulerian approach for the numerical simulation of free-surface flow of a viscoelastic material, J. Non-Newtonian Fluid Mech. 136 (2006) 157–166.

[15] R.G. Owens, C. Chauvière, T.N. Phillips, A locally upwinded spectral technique (LUST) for viscoelastic flows, J. Non-Newtonian Fluid Mech. 108 (2002) 49–71.

[16] Y. Fan, R.I. Tanner, N. Phan-Thien, Galerkin/least-square finite-element methods for steady viscoelastic flows, J. Non-Newtonian Fluid Mech. 84 (1999) 233–256.

[17] M.A. Alves, F.T. Pinho, P.J. Oliveira, The flow of viscoelastic fluids past a cylinder: finite-volume high resolution methods, J. Non-Newtonian Fluid Mech. 97 (2001) 207–232.